Published in final edited form as:
Langmuir. 2012 February 28; 28(8): . doi:10.1021/la203998r.

Association of Poly I:C RNA and Plasmid DNA onto MnO Nanorods Mediated by PAMAM

Brooke Parker-Esquivel[a,*], **Kristin J. Flores**[b,*], **Daniel Louiselle**[b], **Michael Craig**[b], **Lifeng Dong**[c], **Richard Garrad**[b], **Kartik Ghosh**[c], **Adam Wanekaya**[d], **Garry Glaspell**[e], and **Robert K. DeLong**[b,*]

[a]Department of Molecular Biology and Biochemistry, University of Missouri-Kansas City, Kansas City, MO 64110 USA (current address)

[b]Department of Biomedical Sciences, Missouri State University, Springfield, MO 65897 USA

[c]Department of Physics, Astronomy and Materials Science, Missouri State University, Springfield, MO 65897 USA

[d]Department of Chemistry, Missouri State University, Springfield, MO 65897 USA

[e]Department of Chemistry, Virginia Commonwealth University, Richmond, VA 23284 USA

Abstract

In this study, manganese oxide (MnO) nanorods and its association with polyamidoamine dendrimer (PAMAM) and macromolecular RNA were analyzed. Because manganese is found naturally in cells and tissues and binds proteins and nucleic acids, nanomaterials derived from manganese, such as first generation MnO, may have potential as a biocompatible delivery agent for therapeutic or diagnostic biomedical applications. Nucleic acids have a powerful influence over cell processes, such as gene transcription and RNA processing; however, macromolecular RNA is particularly difficult to stabilize as a nanoparticle and to transport across cell membranes while maintaining structure and function. PAMAM is a cationic, branching dendrimer known to form strong complexes with nucleic acids and to protect them from degradation, and is also considered to be a cell penetrating material. There is currently much interest in polyinosinic:polycytidylic RNA (poly I:C) because of its potent and specific immunogenic properties and as a solo or combination therapy. In order to address this potential, here, as a first step, we used PAMAM to attach poly I:C onto MnO nanorods. Morphology of the MnO nanorods was examined by field emission scanning electron microscopy (FESEM) and their composition by energy dispersive X-ray microanalysis (EDX). Evidence was generated for RNA : PAMAM : MnO nanorod binding by a gel shift assay using gel electrophoresis, a sedimentation assay using UV spectroscopy, and zeta potential shifts using dynamic laser light scattering. The data suggest that RNA was successfully attached to the MnO nanorods using PAMAM, and this suggestion was supported by direct visualization of the ternary complexes with FESEM characterizations. In order to confirm that the associations were biocompatible and taken up by cells, MTT assays were carried out to assess the metabolic activity of HeLa cells after incubation with the complexes and appropriate controls. Subsequently, we performed transfection assays using PAMAM:MnO complexes with pDNA encoding a green fluorescent protein reporter gene instead of RNA. The results suggest that the complexes had minimal impact on metabolic activity, were readily taken up by cells, and the fluorescent protein was expressed. From the evidence, we conclude that

[*]Corresponding author: Tel 417-836-5730; Fax 417-836-5588; robertdelong@missouristate.edu.
[*]Authors contributed equally on this work.

Supporting Information Available. This information is available free of charge via the Internet at http://pubs.acs.org/.

complexes of PAMAM:MnO interact with nucleic acids to form associations that are well-tolerated and readily taken up by cells.

Introduction

Nanomaterials exhibit distinctive properties and behaviors when compared to bulk materials, such as large surface areas, high reactivities and energy levels, and unusual optical properties. Knowing the size and shape of the nanomaterial may be just as important for predicting its behavior as knowing its composition.[1–3] With improved techniques for preparation and sophisticated instruments for characterization at the nano level, such as electron microscopy, laser light scattering, and spectroscopy, many fields are able to take advantage of these unique properties for various applications.[3]

The use of nucleic acids as therapeutic agents allows specificity for the target of interest within the cell, allowing influence over such important cell processes as gene transcription and RNA processing, a control not possible with molecules that act extracellularly.[4] Therapeutic nucleic acid examples include short interfering RNA (siRNA), antisense and splice switching oligonucleotides (SSO), and DNA or RNA vaccines. SSO can repair aberrantly-spliced pre-mRNA and in some cases, upregulate gene expression; siRNA can silence a gene by causing targeted mRNA to be degraded, thereby blocking its translation into a protein.[5–10] However, direct treatment of cells with nucleic acids is often unsuccessful, or only transiently effective, due to the difficulties in transporting these molecules across the cell membrane while maintaining their structure and function.[11,12]

At present, although there is great potential, very few nucleic acid therapeutics have been approved for treatments in humans. An exception to this situation is polyinosinic-polycytidylic RNA (poly I:C), chosen for this study as a model therapeutic RNA. Poly I:C is a synthetic, double-stranded RNA that has been used in numerous studies and is well characterized.[13] Its structure is similar to viral RNA, thus making poly I:C useful in immune response studies. Furthermore, poly I:C is a potent vaccine adjuvant, improving vaccine efficacy by stimulating TLR3, and activating interferons and other immune responses against pathogens and even tumors.[14] Clinical trials have shown that poly I:C improves traditional chemotherapeutic drug effectiveness when used concurrently.[15] One company, Hemispherx Biopharma Inc., is currently conducting human clinical trials testing its poly I:C drug version, Ampligen, for effects in a variety of diseases and disorders. Ampligen on its own, or in combination with other drugs, has shown promise for treatment of HIV, chronic fatigue syndrome, renal cell carcinoma, and malignant melanoma.[16]

DNA attached to gold or tungsten nanoparticles, then delivered biolistically via gene gun, has proven to be an effective vaccination method.[17] However, such an approach damages tissues, can be used on skin or other accessible tissues only, and is probably not amenable for macromolecular RNA, siRNA, or SSO delivery.[18] Using nanomaterials rather than microparticles may offer a delivery advantage or, by exploiting the unique optical, electrical, or magnetic properties exhibited by some nanomaterials, find utility in biosensing and imaging applications.[19,20] Moreover, it has been demonstrated that attaching DNA to nanoparticles, using protamine adapter molecules or tetraalkylammonium ligands, offers enhanced nucleic acid stability, permitting the nucleic acid cargo to withstand temperature, chemical, and even nuclease degradation, in some cases for weeks or months.[17,21,22] Thus, a new generation of biomedical tools has been born with the binding of nucleic acids onto nanomaterials, creating improvements in disease treatment and diagnosis. Extensive research has been performed on optimizing gold nanomaterials[21–23] and more recently, carbon nanotubes,[24] to interact with nucleic acids and be biocompatible with cells; however,

as mentioned above, different materials, having varying size, shape, or elemental composition, exhibit disparate behavior, and what is true for gold may not be the case for other nanomaterials.

Here we chose to study manganese oxide nanorods as potential nucleic acid delivery agents. It is understood that the manganese and oxygen atoms in the nanorods may exist in different molar ratios; however, for convenience, MnO will be used throughout to represent the general term manganese oxide. Manganese ions are found naturally in cells and tissues of humans and other organisms and are known to interact with different biomolecules and nucleic acids.[25,26] Therefore, nanomaterials derived from manganese have the potential to be a very biocompatible material although few studies have investigated this effect[27] and even fewer have investigated nucleic acid attachment to manganese nanomaterials. We showed previously that MnO nanorods were not toxic to cells by treating three different cell lines with a range of MnO nanorod concentrations.[28] In addition to being well tolerated, the MnO nanorods unexpectedly seemed to localize on the cell surface.[28]

In preliminary experiments, dynamic laser light scattering (DLLS) and zeta potential measurements demonstrated that the manganese nanorods are negatively charged in water. Thus, the MnO would not be expected to interact directly with nucleic acids, which are predominantly negatively charged due to their phosphodiester backbone. For this and other reasons described below, we chose a cationic, branching dendrimer, polyamidoamine (PAMAM), to attach RNA onto the manganese oxide nanorods. PAMAM dendrimers are three-dimensional, arborized polymers first created by Baker and Tomalia ostensibly for gene delivery.[29] The highly-branched structure maximizes surface area and exposes surface groups for interactions, making the dendrimers highly reactive and suitable for binding a variety of molecules.[30] This versatility and specificity has made dendrimers a popular choice for such uses as drug delivery, diagnostics, tumor detection, and gene therapy.[31–33] Higher generation dendrimers are more positively charged than lower generations. Toxicity increases with increasing generations of the cationic dendrimers, however multiple studies have demonstrated that generation 5 PAMAM, such as the one used in this study, is non-toxic and effectively delivers nucleic acids into cells.[38,39] Smaller generation cationic PAMAM dendrimers (≤ generation 6),[34] such as the generation 5 used in this study, are thought to act similarly to histones and have been exhaustively shown to form complexes with DNA and RNA.[12,35,36] PAMAM dendrimer has several other advantages, including protecting RNA from nuclease degradation[37], and is also considered a cell-penetrating molecule[38,39] and has been shown in other studies to deliver DNA or RNA oligonucleotides into cells.[33–39] The positively-charged terminal amines of the dendrimer are thought to bind to the negatively-charged phosphate backbone groups of the nucleic acid, facilitating an electrostatic interaction between the dendrimers and nucleic acid.

In this study, we hypothesized that PAMAM, being a multiple-branched highly cationic polymer, could be used to attach anionic nucleic acids, notably poly I:C RNA, onto MnO nanorods. We reviewed recently the interactions of gold nanomaterials with proteins, where for these types of nano-assemblies, a surface interaction is achieved by known electrostatic mechanisms.[41] Therefore, we were interested in creating a similar yet distinct assembly, bringing together the RNA, PAMAM and MnO. As described herein, we characterized the size, shape, and composition of the manganese nanorods using field emission scanning electron microscopy (FESEM) and energy-dispersive X-ray microanalysis (EDX). Dynamic laser light scattering, UV/Vis Nanodrop spectroscopy, sedimentation analyses, and electrophoretic gel mobility shift were used to demonstrate association of the macromolecular RNA via PAMAM to the MnO nanorods, and this association was supported by images obtained from the FESEM. To investigate the biocompatability of the RNA:PAMAM:MnO complexes, an MTT assay was performed in HeLa cells. This is a

colorimetric assay based on the reduction of water soluble yellow MTT (3-(4,5-dimethylthiazol-2-yl)-2,5-diphenyltetrazolium bromide) to insoluble purple formazan. In order to confirm cellular uptake of the complexes, transfection assays were carried out using plasmid DNA with a green fluorescent protein (GFP) reporter gene in place of the RNA. As described below, ternary complexes of RNA:PAMAM:MnO were formed that may be a powerful new bionanomaterial to explore for therapeutic or diagnostic applications, including their future potential as a macromolecular RNA delivery reagent.

Experimental Section

MnO Nanorod Preparation

The manganese oxide nanorods were synthesized by the standard K-birnessite procedure of hydrothermally treating a mixture of $KMnO_4$-$MnCl_2$ in a highly-concentrated KOH solution.[2] Briefly, $KMnO_4$ was dissolved in water and a high concentration of KOH was added while stirring. Aqueous $MnCl_2$ was then added to this solution and allowed to cool with continuous stirring. Subsequently, the resultant black slurry was sealed in a stainless steel autoclave and placed in an electric oven at 175 °C for 2 days. Once cooled, the dark gray solid was rinsed with water to remove KOH residue and air dried.[2]

FESEM imaging and X-ray microanalysis

A 0.1 mg aliquot of the dry MnO nanorod powder was suspended in 1 mL of Type I water (22 MΩ, RNase free) and centrifuged at 15 k rpm for 5 min; subsequently, the supernatant was removed, 1 mL of Type I water added, and the preparation was vortexed and centrifuged again at 15k rpm for 10 min. This washing sequence was repeated an additional 3 times, and the preparation was sonicated for 5 min. A sample of this washed preparation was subsequently deposited with a glass micropipette on the beveled depression side of a 3 mm diameter silicon nitride grid (Ted Pella, Inc.), having a window area of 0.5 mm × 0.5 mm, a membrane thickness of 50 nm, and treated to be hydrophilic. The sample was permitted to air dry in a desiccators for 3 hr prior to inspection.

The silicon nitride grid was subsequently loaded into the specimen chamber of an FEI Quanta 200 FESEM, equipped with an Oxford Inca EDX system and a 20 mm^2 window silicon drift detector (SDD), and plasma cleaned in the chamber for 10 min immediately prior to examination. All images were acquired digitally at 30 kV acceleration potential in the secondary electron (SE) mode and the following scanning transmission electron microscopy (STEM) modes: bright field (BF) and high-angle annular dark-field (HAADF) mode. Dimensional measurements of particles were made directly from resultant digital images.

Preparation of RNA:PAMAM:MnO conjugates for ultrastructural examination was performed as follows. Dry MnO nanorod powder was washed as described above, then the RNA:PAMAM:MnO conjugate was prepared as described below in the zeta potential shift analysis section. Aliquots of the ternary complexes were washed 3 times in cold 80% ethanol; subsequently, 0.5 μl of the washed preparation was deposited on an ultrathin carbon film over holey carbon supported on 400 mesh copper grids (Ted Pella, Inc.), air dried, then examined with the FEI FESEM at 30 kV in the secondary electron detection mode.

Zeta potential shift analysis by dynamic laser light scattering

DLLS analysis was performed on a Malvern Zetasizer Nano series ZS-90, model ZEN3690 (Worcestershire, UK) and all readings were taken in triplicate. The MnO nanorod sample was prepared by adding 0.25 mg of the MnO nanorod dry powder to 1 mL of water obtained from a Millipore Synergy UV filtration system (Molsheim, France), sonicating for 7 min,

then vortex mixed for 20 sec. All water used in this and subsequent analyses (described below) was Type I water (22 MΩ, RNase free, ultra-filtered).

Generation 5 PAMAM dendrimer was used with a 1,12-diaminododecane core, in a 10% w/v solution in methanol from Sigma-Aldrich (St. Louis, MO). MnO and PAMAM samples used for DLLS analysis were prepared as follows. A 0.25 mg/mL solution of MnO was set aside and 5 μL PAMAM stock solution was added to 245 μL water. Equal parts of the MnO and PAMAM solution were combined, and this solution was vortexed for 20 sec before taking the DLLS measurements.

Poly I:C RNA, at a 5.1 mg/mL stock concentration from Sigma-Aldrich (St. Louis), was used for all RNA experiments. Samples of MnO with PAMAM and poly I:C RNA were prepared as follows. A 0.25 mg/mL MnO solution was set aside and 5 μL PAMAM stock solution was added to 245 μL water. To the PAMAM solution, 2.5 μL poly I:C RNA stock solution was added and vortexed. Equal parts of the 0.25 mg/mL MnO solution and the PAMAM:poly I:C solution were combined. The sample was vortexed for 20 sec before taking the zeta potential measurements.

Ultraviolet spectroscopy of sedimentation assay

This assay was performed similarly to our previous work with gold particle-bound nucleic acid[17]. For ultraviolet spectroscopy, we used a NanoDrop 2000 Spectrophotometer with a Xenon flash lamp light source and 2048-element linear silicon CCD array detector from Thermo Fisher Scientific (Wilmington, DE). As a reference to poly I:C RNA UV absorbance and to check the sensitivity of the NanoDrop spectrophotometer to changes in poly I:C concentration, a gradient of poly I:C concentrations was measured. For the poly I:C concentration gradient spectrum, 1 μL poly I:C stock solution was added to a microcentrifuge tube with 1000 μL water and vortexed for 15 sec. A 1 μL sample was taken from this solution and placed directly on the NanoDrop pedestal for a UV spectrophotometry measurement using the nucleic acid analysis stock program. The poly I:C 2/1000 sample was prepared by adding 1 μL poly I:C stock solution to the previous 1/1000 sample. Again, the sample was vortexed for 15 sec and a UV absorbance measurement was taken from 1 μL of this new poly I:C concentration. Subsequent poly I:C samples were prepared and measured in the same manner by adding the indicated amount (3/1000, 5/1000, and 6/1000) of poly I:C to the preceding sample. These samples are indicated in Fig. 4 as 1/1000, 2/1000, 3/1000, 4/1000, 5/1000, and 6/1000, a notation that refers to the volume of stock poly I:C added in μL to 1000 μL spectral grade water.

For the PAMAM and PAMAM:MnO UV spectra, the PAMAM only sample was prepared by adding 1 μL PAMAM stock solution to 99 μL water. The PAMAM:MnO sample was prepared by adding 1 μL PAMAM stock solution to 99 μL of a 0.125 mg/mL MnO solution. Subsequently, UV absorbance measurements were taken for these samples.

For binding comparisons between RNA:PAMAM and RNA:PAMAM:MnO, the samples were prepared as follows. For the PAMAM:RNA sample, 2 μL PAMAM stock solution were added to 198 μL water and vortexed for 10 sec. To this, 1 μL poly I:C RNA stock solution was added and vortexed for 10 sec. A 2 μL sample was drawn from this sample and measured using the nucleic acid stock program. The PAMAM plus poly I:C sample was then centrifuged at 21,000 rcf for 7 min at 10 °C, and 2 μL was immediately drawn from the supernatant and measured.

For the RNA:PAMAM:MnO sample, 2 μL PAMAM stock solution was added to 98 μL water and vortexed for 10 sec. To this volume, 1 μL poly I:C stock solution was added and vortex mixed for 10 sec. Next, this PAMAM plus poly I:C solution was added to 100 μL of

a 0.25 mg/mL MnO solution and vortexed for 10 sec. For the RNA only sample, 1 μL poly I:C RNA stock solution was added to 200 μL water and vortexed for 10 sec. A 2 μL sample was taken from each and measured on the NanoDrop pedestal using the same program as above, and the remaining samples was centrifuged at 21,000 rcf at 10 °C for 7 min. A 2 μL sample was immediately taken from the supernatant of each sample and measured.

In order to carry out the transfection assays using plasmid DNA with a reporter gene, we had to verify that the PAMAM:MnO complexes also associated with plasmid DNA. Sedimentation assays were used to confirm this association. For the pDNA:PAMAM:MnO sample, 2 μL PAMAM stock solution was added to 98 μL water and vortexed for 10 sec. To this volume, 1 μL of 5 mg/mL gWiz-GFP High Expression Reporter Plasmid stock solution from Aldevron (North Dakota) was added and vortex mixed for 10 sec. Next, this PAMAM plus pDNA solution was added to 100 μL of a 0.25 mg/mL MnO solution and vortexed for 10 sec. For the pDNA only sample, 1 μL gWiz-GFP pDNA stock solution was added to 200 μL water and vortexed for 10 sec. A 2 μL sample was taken from each and measured on the NanoDrop pedestal using the same program as above, and the remaining samples was centrifuged at 21,000 rcf at 10 °C for 7 min. A 2 μL sample was immediately taken from the supernatant of each sample and measured.

Gel shift assay

For the gel shift assay, samples were prepared as follows. For the poly I:C RNA sample, 1 μL poly I:C stock solution was added to 100 μL water and vortexed for 10 sec; 20 μL were used for the sample. For the PAMAM sample, 1 μL PAMAM stock solution was added to 50 μL water and vortexed for 10 sec, and 20 μL were used for the sample. For the first PAMAM:RNA sample, 6 μL PAMAM stock solution was added to 294 μL water and vortexed for 10 sec; 3 μL poly I:C stock solution was added and vortexed for an additional 10 sec. A 20 μL sample was used. For the second PAMAM:RNA sample, 4 μL PAMAM stock solution was added to 96 μL of water and vortex mixed for 10 sec. To this aliquot, 2 μL of poly I:C stock solution was added and vortexed for 10 sec; 20 μL were used as the sample. For the RNA:PAMAM:MnO sample, 6 μL PAMAM stock solution was added to 144 μL water and vortexed for 10 sec. To this solution, 3 μL poly I:C stock solution was added and vortexed for 10 sec. Subsequently, a 0.5 mg/mL MnO in water suspension was prepared and 150 μL was taken from this and added to the PAMAM and poly I:C solution and vortexed for 10 sec. A 20 μL sample was used.

Finally, the PAMAM:MnO sample was prepared by adding 2 μL PAMAM stock solution to a 100 μL sample containing 0.25 mg/mL MnO and vortexed for 10 sec. A 20 μL sample was used. All samples were mixed with 2 μL of loading dye and loaded in a 2% agarose gel. The gel was made with 1X TAE buffer containing 1 μL of 10 mg/mL ethidium bromide and run at 90 V for 35 min in 1X TAE buffer. The gel was then soaked in a 1% ethidium bromide staining solution for 10 min before being imaged under UV light using a Kodak Gel Logic 200 Imaging System (Rochester, NY).

MTT (3-(4, 5-dimethylthiazol-2-yl)-2,5-diphenyltetrazoliumbromide) assay

All cell culture work and related assays were performed under the laminar flow hood, using sterile technique. HeLa cells from ATCC (Virginia), suspended in 1X phenol red-free DMEM/10% FBS/1% penicillin and streptomycin from Sigma Aldrich (St. Louis), were seeded in 96-well Cellstar cell culture plates in a volume of 100 μL per well. The plates were incubated at 37° C overnight with 5% CO_2, to allow the cells to attach.

Triplicate samples of RNA:PAMAM:MnO and pDNA:PAMAM:MnO conjugates were made as previously described in Type I water, only the volumes were scaled up 4X. The

samples were centrifuged at 21,000 rcf for 7 min at 10 °C, and 2 μL was immediately drawn from the supernatant and the UV absorbance was measured to confirm association of nucleic acids, PAMAM, and nanorods. The supernatant was carefully removed from each tube using vacuum suction, and the pellets were resuspended in 800 μL of serum-free, phenol red-free DMEM from Sigma-Aldrich (St. Louis).

Triplicate samples of MnO only were prepared from 800 μL of the 0.25 mg/mL stock solution, which was centrifuged at 21,000 rcf for 7 min at 10 °C to pellet the nanorods. The supernatant was carefully removed from each tube using vacuum suction, and the pellets were resuspended in 800 μL of serum-free, phenol red-free DMEM. From these solutions, 100 μL was added to each corresponding well. A set of control wells contained only cells and serum-free, phenol red-free DMEM. The plates were incubated for 24 hours at 37° C with 5% CO_2.

After incubation, the medium was removed and the cells were washed with sterile 1X PBS to remove any residual MnO or conjugates, to avoid any interference with the absorbance readings. To each well, 100 μL of fresh serum-free, phenol red-free medium was added, along with 10 μL of a 12 mM MTT stock solution, prepared by adding 1 mL of sterile 1X PBS to 5 mg of 12 mM MTT (3-(4, 5-dimethylthiazol-2-yl)-2,5-diphenyltetrazoliumbromide) from Invitrogen (Carlsbad, California). One well served as a negative control, containing only 100 μL of medium and 10 μL of MTT. The plates were incubated for 4 hours at 37° C with 5% CO_2.

After incubating with MTT, all but 25 μL of medium was removed from each well. Using a multichannel pipetter, 50 μL of DMSO was added to each well and mixed by pipetting. The plates were incubated at 37° C for 10 minutes to allow the DMSO to solubilize the formazan. The samples were mixed again by pipetting, and the absorbance reading was taken at 562 nm using the EL_x800 Universal Microplate Reader by Bio-Tek Instruments, Inc. (Winooski, Vermont).

To investigate the cellular effects of longer-term exposure to MnO, MTT assays were performed with various incubation times, ranging from 12 to 48 hours. After plating the HeLa cells using the same protocol described above, the cells were incubated overnight at 37° C with 5% CO_2, to permit cell attachment. The medium was removed from each well, and replaced with 100 μL of 0.25 mg/mL MnO stock solution made with serum-free, phenol red-free DMEM from Sigma-Aldrich, rather than Type I water. Control wells contained medium only.

The plates were incubated at 37° C with 5% CO_2 for 12, 24, 36, or 48 hours. The same protocol detailed above was followed for the remainder of this MTT assay.

An MTT assay was also performed to investigate the effects of varying concentrations of PAMAM on the metabolic activity of HeLa cells. The cells were seeded in the 96-well plates and incubated for 24 hours, as previously mentioned.

The PAMAM concentrations used for this assay were 1, 1.5, 2, 2.5, and 3 μL/mL. The PAMAM only samples were made by adding PAMAM in the appropriate concentration directly to the serum-free, phenol-free DMEM. The PAMAM:MnO, RNA:PAMAM:MnO, and pDNA:PAMAM:MnO samples were prepared in Type I water, pelleted, and resuspended in medium, as described previously. The same protocol detailed above was followed for this MTT assay.

Transfection assay

For the transfection assays, all samples were ran in duplicate. HeLa cells, suspended in 1X phenol red-free DMEM/10% FBS/1% penicillin and streptomycin from Sigma Aldrich, were seeded in Nunc Lab-Tek 4-well chamber slide with cover (Sigma Aldrich), in a volume of 500 μL per well. The chamber slides were incubated at 37° C overnight with 5% CO_2, to permit cell attachment. After overnight incubation, the cells were visualized by compound light microscope to verify approximately 50% confluence. The medium was removed using vacuum suction.

The first well, intended to serve as the negative control, contained PAMAM:MnO only. This sample was made by adding 6 μL of PAMAM stock solution to 294 μL of Type I water. This was vortexed for 10 seconds, and added to 300 μL of 0.25 mg/mL stock solution. The sample was vortexed for 10 seconds, the absorbance was read using the NanoDrop, and then the sample was centrifuged at 21,000 rcf at 10 °C for 7 min. After spinning, the absorbance was read again to confirm loss from the supernatant, which was then removed by vacuum suction. The pellet was resuspended in 600 μL Opti-MEM I Reduced Serum Medium from Invitrogen. From this sample, 500 μL was removed and added to the first well.

The second well contained PAMAM:pDNA only. This sample was made by adding 6 μL of PAMAM stock solution to 594 μL of Type I water. This was vortexed for 10 seconds, and 3 μL of 5 mg/mL gWiz-GFP High Expression Reporter Plasmid stock solution was added. The sample was vortexed for 10 seconds, the absorbance was read using the NanoDrop, and then the sample was centrifuged at 21,000 rcf at 10 °C for 7 min. After spinning, the absorbance was read again to confirm loss from the supernatant, which was then removed by vacuum suction. The pellet was resuspended in 600 μL Opti-MEM I Reduced Serum Medium from Invitrogen. From this sample, 500 μL was removed and added to the second well.

The third well, which was intended to serve as a positive control, contained pDNA:Lipofectamine only. This sample was made by adding 3 μL of 5 mg/mL gWiz-GFP High Expression Reporter Plasmid stock solution to 100 μL Opti-MEM I Reduced Serum Medium, followed by the addition of 1.5 μL Lipofectamine reagent from Invitrogen. The sample was mixed gently by inversion, and allowed to incubate at room temperature for 30 minutes to allow the formation of pDNA:Lipofectamine complexes, followed by the addition of 500 μL Opti-MEM I Reduced Serum Medium. From this sample, 500 μL was removed and added to the third well.

The fourth well contained the conjugates of pDNA:PAMAM:MnO complex. This sample was made by adding 6 μL of PAMAM stock solution to 294 μL of Type I water. This was vortexed for 10 seconds, and 3 μL of 5 mg/mL gWiz-GFP High Expression Reporter Plasmid stock solution was added. The sample was vortexed for 10 seconds, and then added to 300 μL of 0.25 mg/mL stock solution, and vortexed again for 10 sec. The absorbance was read using the NanoDrop, and then the sample was centrifuged at 21,000 rcf at 10 °C for 7 min. After spinning, the absorbance was read again to confirm loss from the supernatant, which was then removed by vacuum suction. The pellet was resuspended in 600 μL Opti-MEM I Reduced Serum Medium from Invitrogen. From this sample, 500 μL was removed and added to the fourth well.

The chamber slides were allowed to incubate for 24 hours at 37° C with 5% CO_2. After this incubation, the medium was removed with vacuum suction, and replaced with 500 μL 1X phenol red-free DMEM/10% FBS/1% penicillin and streptomycin from Sigma Aldrich, and allowed to incubated for another 24 hours at 37° C with 5% CO_2.

Following incubation in serum-containing medium, the medium was removed using vacuum suction. The chambers were then split apart from the microscope slide. Mounting medium was applied to the microscope slide to protect the samples against desiccation, and a cover slip was placed on the microscope slide. After a brief drying period of 10 minutes, the cell samples were viewed using a mercury lamp-powered Olympus BX60 fluorescent microscope. Cells were viewed using brightfield microscopy and fluorescent microscopy using a GFP-specific filter. Images were acquired via a Q-Imaging Retiga Ex camera attached to the microscope. Image Pro Plus software employed to save the images automatically, calibrated the exposure times for each image for optimal clarity.

Results

MnO nanorod morphology using FESEM

Figure 1a depicts the unwashed MnO powder in secondary electron (SE) image mode. The aggregate appeared to consist of numerous flattened rods with rounded ends, a shape that we designated as a platelet, or spatula, shape. When dispersed on a silicon nitride membrane, however, the array appeared to be heterogeneous, with at least three classes of particles discernable. One class of particles consisted of large spatulas (length range: 720 nm – 1.4 μm; width range: 50 nm – 172 nm) (Figure 1b, 1c). Another class of MnO nanorods appeared to be small spatulas (length range: 330 nm – 1.0 μm; width range: 42 nm – 75 nm) (Figure 1c). Still another class of MnO particles were the filaments (length range: 4 μm – 5 μm; width range: 19 nm – 25 nm) (Figure 1b, 1c, 1d). We were unable to visualize the cross-sectional aspect of any filament, and therefore, were unable to identify the cross-sectional filament shape as being circular, flattened like the spatulas, or some other shape.

MnO nanorod composition using EDX microanalysis

Energy-dispersive X-ray (EDX) spot analysis of a single large spatula is demonstrated in Figure 2a. The resultant spectrum (Figure 2b) revealed the presence of elements anticipated for this preparation: Mn and O are derived from the designated nanorod; Si and N (peak not labeled), support substratum; Al, specimen holder.

RNA:PAMAM:MnO complex morphology using FESEM

Evidence for an association among the RNA, PAMAM, and MnO, as revealed by electron microscopy, is shown in Figure 3. Figure 3a demonstrates the morphology of the ethanol-washed, RNA:PAMAM:MnO complex. The components of the complex associated into either discrete solid plaques, or as nodules projecting from a solid sheet of the complex. Within a patch (Figure 3a), one can observe MnO nanorods embedded in the association matrix. At higher magnifications (Figure 3b), individual nanorods appeared to be bound to one another by a membrane-like residuum, an obvious example of which is indicated by the arrow in Figure 3b.

DLLS zeta potential shifts

DLLS zeta potential measurements (Figure 4 and Table 1) demonstrated that the negatively-charged manganese oxide nanorod surfaces became positively charged when PAMAM was added, indicating that PAMAM binds to the nanorod surface. A sample with RNA:MnO was analyzed, but because MnO and RNA do not interact without the PAMAM, there was no shift. Samples with PAMAM or RNA alone were also analyzed; however, since no nanoparticles are present in these samples, the DLLS does not record a shift. For simplicity, these samples were omitted from Figure 4.

As RNA was added to the PAMAM:MnO complex, the charge changed again, becoming less positive, suggesting possible binding of the anionic nucleic acid to the nanorod-

dendrimer complex (Figure 4 and Table 1). Median values are represented in Figure 4 and average values with standard deviations are shown in Table 1.

UV spectroscopy of sedimentation assay

The poly I:C concentration gradient demonstrated an expected increase in absorbance as the poly I:C concentration increased. As seen from the spectrum, the poly I:C had an absorbance peak circa 248 nm and a less defined peak around 270 nm (Figure 5a). The peak around 270 nm corresponds to the cytidylic chain of the poly I:C, and the peak at 248 nm corresponds to the inosinic chain.[42,43]

The UV absorbance maximum of the generation 5 PAMAM was approximately 210 nm. The MnO nanorods did not exhibit UV absorbance, yet when combined with PAMAM, the PAMAM:MnO spectrum demonstrates a shift to a PAMAM absorbance maximum around 205 nm (Figure 5b), indicating an interaction of PAMAM with the nanorods.

Sedimentation assays were performed to confirm RNA:PAMAM:MnO binding using UV spectroscopy, similar to our previous work.[17] Because we planned to do transfection assays using plasmid DNA with a GFP reporter gene, we included binding analysis of pDNA:PAMAM:MnO in the sedimentation assays. Even after centrifugation, neither RNA by itself, pDNA by itself, nor PAMAM by itself, will form a pellet or sediment; therefore, their UV absorbance will be the same before and after centrifugation. For these molecules to sediment, they must form a complex with another molecule. For this reason, the UV spectrum from RNA, pDNA, and PAMAM alone were excluded from Figure 6 for simplicity. If a complex is formed and subsequent sedimentation occurs, there will be a decrease in UV absorbance due to the loss of the RNA, DNA, or PAMAM in the solution. In addition, when the nucleic acid analysis program on the NanoDrop 2000 is used, an added sedimentation indicator is that the instrument estimates the nucleic acid concentration in the solution. Thus, in addition to analyzing UV absorbance decreases, one can analyze decreases in nucleic acid concentration.

The sedimentation assay results (Figure 6) show a marked decrease in RNA and DNA concentration and UV absorbance of the supernatant after centrifugation with the manganese oxide nanorods and PAMAM. This observation indicates that the RNA and DNA both bound to the PAMAM:MnO complex and so were sedimented as a RNA:PAMAM:MnO complex (Figure 6a and Table 2) or a pDNA:PAMAM:MnO complex (Figure 6b and Table 2), respectively, during centrifugation. Although sedimentation reactions involving RNA:PAMAM and pDNA:PAMAM without the MnO nanorods also exhibited a pronounced decrease in RNA and pDNA concentration and UV absorbance after centrifugation, these reductions were not as dramatic as when the manganese oxide nanorods were used. These data indicate that binding of RNA and pDNA to the manganese oxide nanorods is mediated by PAMAM (Figure 6 and Table 2).

Gel shift assay

A gel shift assay was executed to confirm RNA:PAMAM:MnO complexation (Figure 7). RNA migration through the gel was inhibited in all wells containing PAMAM, showing that the two molecules form a complex that we and many others have observed previously.[33–39] Neither the PAMAM (lane 2) nor PAMAM:MnO (lane 6) stain with ethidium bromide. Interestingly, for lane 5, containing the ternary complex RNA:PAMAM:MnO, no difference in migration was observed; however, a loss of fluorescence intensity was shown in this lane. This observation is consistent with a loss of ethidium binding sites in the RNA or dye exclusion as a function of the RNA complexing with the PAMAM:MnO, which we have seen previously for protamine binding to RNA in nanoparticle formation.[17] A sample

containing RNA:MnO was analyzed for a gel shift, but because MnO and RNA do not interact without a mediator, no shift was visible.

MTT Assay

A previous cytotoxicity study using three cell lines suggested the potential of MnO to be well-tolerated by cells.[27] Our MTT assays using HeLa cells confirmed that study. The data shown in Figure 8a suggests that a 24 hour incubation with conjugates of RNA:PAMAM:MnO and pDNA: PAMAM:MnO have very little effect on the ability of HeLa cells to metabolize the yellow MTT to purple formazan, which was measured by absorbance (Figure 8). The data in Figure 8b indicates that cells incubated in MnO for up to 48 hours retained a significant ability to metabolize the MTT to formazan. The slight decrease in absorbance measurements for the cells incubated in MnO is similar to the slight gradual decrease in absorbance measurements for the control. This result is likely due to the cells being in serum-free medium for longer periods of time.

Another MTT assay was used to study the effects of various concentrations of PAMAM on the metabolic activity of HeLa cells. There are numerous studies on the cell penetrating activity of PAMAM dendrimers and their ability to carry cargo through the plasma membrane.[34–41] Several of these studies suggest that PAMAM is potentially cytotoxic, though this effect can be reduced by complexing the PAMAM with other molecules or functionalizing the surface of the dendrimer.[34–41] The data from this MTT assay supports those findings (Figure 9), as PAMAM alone, even at low concentrations, caused a significant reduction in metabolic activity of HeLa cells. When PAMAM was associated with MnO nanorods, the ability of the HeLa cells to metabolize the MTT had a notable increase.

Interestingly, when the PAMAM:MnO conjugates were associated with nucleic acids, either RNA or DNA, the metabolic activity of the HeLa cells was substantially higher at PAMAM concentrations of 2 μL/mL and below. We conclude that the nucleic acids and MnO bound to PAMAM at lower concentrations provide a protective effect for the cells. While this reduction in cytotoxicity is desirable, we had to confirm that the nucleic acids do not block the cell penetrating properties of PAMAM. Therefore, we determined that 2 μL/mL was the appropriate PAMAM concentration for our work, because this concentration permits the cells to retain most of their metabolic activity while allowing the PAMAM to penetrate the plasma membrane, as shown in the transfection assay (Figure 10).

Transfection assays

Having already confirmed that the complexes formed with PAMAM:MnO and nucleic acids were not cytotoxic to HeLa cells, we wanted next to investigate their transfection ability. The PAMAM:MnO only sample, which served as the negative control, demonstrated no visible fluorescence, which is to be expected since there is no pDNA with GFP reporter gene in this sample. Because the images from this sample exhibited no fluorescent signal, they were not included in Figure 10.

The image of the cells incubated with pDNA:PAMAM (Figure 10a) shows relatively little fluorescence. This result was expected, since we know from the literature that PAMAM is a cell penetrating molecule that can carry its cargo through the plasma membrane.[34–41] The image of the cells incubated with the Lipofectamine:pDNA (Figure 10b) shows several cells displaying low fluorescence, and a few that demonstrate high expression of the GFP. Although Lipofectamine is a common transfection agent in the lab, it can also be relatively cytotoxic and often provides low transfection efficiency.[45–46] The image of the cells incubated with the pDNA:PAMAM:MnO complexes (Figure 10c) showed more cells with

significantly higher expression of the GFP. The expression is much more consistent, a result that we suggest is due to minimal toxicity of the pDNA:PAMAM:MnO complexes, as opposed to the pDNA:PAMAM and pDNA:Lipofectamine. When considering the results from our MTT assay in Figure 8, we conclude that the cells incubated with the pDNA:PAMAM:MnO complexes do not require significant time to recover from the transfection.

Discussion

Our data suggest that we have successfully used PAMAM to attach macromolecular RNA to MnO nanorods. We first characterized the morphology of the MnO nanorods using FESEM. Manganese oxide composition of the nanorods was confirmed using EDX. This approach produced high quality nanoscale images from which the nanorod morphology was deduced. In a similar fashion, FESEM inspection of solid, discrete patches or nodules of the ternary complexes revealed a morphology indicating MnO nanorods embedded in, or interconnected by, an association matrix.

The zeta potential of the MnO nanorods was determined using DLLS. Zeta potential is similar to surface charge and can be used to determine solution stability and detect particle adsorption. Particles in solution with a charged surface will attract oppositely charged ions from the solution that bind to the particle surface. As the particle moves, the layer of highly attracted ions will move with the particle, while non-attracted ions remain in the bulk solution. The difference between the ions bound to the surface and those in the bulk solution is considered the zeta potential.[44] The manganese oxide composition implied the potential to be well tolerated by cells, and a prior cytotoxicity study testing three different cell lines confirmed this potential.[28] The negative zeta potential made the idea of attaching anionic nucleic acids directly to the MnO surface unlikely; however, it was hypothesized that nucleic acids could be attached if mediated by some cationic binding agent. The cationic binding agent selected was PAMAM dendrimer. Zeta potential shift analysis using DLLS supported hypothetical RNA:PAMAM:MnO nanorod association.

Before a new nanomaterial can be used as a delivery agent for macromolecular RNA, it is first necessary to demonstrate its interaction with the nucleic acid. MnO nanorod binding to RNA via PAMAM was confirmed by agarose gel electrophoresis, demonstrating a gel shift of the RNA:PAMAM or a change in staining intensity consistent with RNA:PAMAM:MnO ternary species. In addition, a sedimentation assay using ultraviolet spectroscopy was performed. In this assay, we compared the nucleic acid UV absorbance of a sample before and after centrifugation. Nucleic acids in solution will not sediment or form a pellet when centrifuged; therefore, large decreases in nucleic acid UV absorbance indicate binding, and subsequent sedimentation, of the nucleic acid complexes.

Finally, although FESEM images revealed a heterogeneous mixture of lengths and widths, the MnO materials generally had at least one dimension under 100 nm, and so were labeled nanorods. Because many cell processes operate at the nano level, the nano sized rods may be more successful as cellular delivery agents as compared to larger materials. However, benefits and limitations of the rod morphology, compared to other morphologies, are unknown and need to be addressed. As stated previously, the cationic terminal groups of PAMAM have been shown to bind anionic nucleic acids tightly[12,35,36] and even offer protection from degradation.[37] Furthermore, it was assumed that as long as the overall charge of the RNA:PAMAM complex was slightly positive, it should bind to the negatively charged MnO nanorods. In addition to being a cationic “glue” for the binding of RNA to the nanorods, PAMAM has been demonstrated to interact with cell membranes, allowing the dendrimer and any cargo it may carry to enter the cell.[34–41], and our transfection assays

provide further evidence for cellular uptake. A visible ultrastructural manifestation of the RNA:PAMAM:MnO complex supports the indirect evidence, discussed above, for that association. The data from the transfection assay support this observation, showing that the PAMAM:MnO complex carried the pDNA with the reporter gene through the plasma membrane, ultimately leading to expression of the green fluorescent protein in the cells.

Nucleic acids have the potential to be powerful therapeutic agents because of their sequence specificity and ability to interact with targeted DNA or RNA and manipulate cell processes such as transcription, splicing, and translation at the molecular level.[4–7,12] While metal containing inorganic nanoparticles, especially gold-based systems are widely used for gene delivery, comparatively little work has been reported for manganese nanomaterials. Most recently a similar alkyl-PEI2k-MnO/siRNA nanocluster system was reported[47], which our approach and the results presented herein both confirm and extend. Although this area of study could still be considered in its infancy, some hypothesize that nucleic acid therapeutics will one day replace traditional drug treatments for almost any disorder caused by molecular dysfunction.[4] The first antisense drug, Formavirsen, was approved for human use in 1998 as an antiviral treatment for cytomegalovirus.[8] Other nucleic acid drugs, like Ampligen, derived from the poly I:C used in our studies, are in development or being tested in humans.[14–16] However, the clinical progress for RNA macromolecules has been slowed, as generally acknowledged by the inability to identify a nanoparticle complex with favorable stabilization and delivery properties.[48] Here, we have taken a significant first step in that direction by associating poly I:C onto manganese nanorods via PAMAM.

Conclusions

In summary, based on evidence provided by DLLS, sedimentation coupled to UV/Vis spectroscopy, gel shift assays, and direct visualization by scanning electron microscopy, poly I:C RNA has been successfully attached to MnO nanorods by PAMAM. Given the well-known membrane penetrating and cell delivery potential of PAMAM, which is supported by our transfection assay, combined with the MnO nanorod structure being well tolerated by several human cell lines[28], which is supported by our MTT assays, the RNA:PAMAM:MnO ternary complex may have great future potential as a novel poly I:C or possibly siRNA delivery vehicle. Furthermore, given the interest clinically in poly I:C as a potent and safe immunogen in humans, the potential for MnO being compatible with, and prolonging the structure-function of, macromolecular RNA is also promising. This potential remains important to address in future studies.

Acknowledgments

This investigation was supported by the National Science Foundation (DMR-0821159) and by a research grant from the National Cancer Institute (1 R15 CA139390-01) to AW, KG, RG and RKD.

References and Citations

1. Cao, G. Nanostructures & Nanomaterials, Synthesis, Properties & Applications. London: Imperial College Press; 2004. Chapter 1.
2. Liu Z, Ma R, Ebina Y, Takada K, Sasaki T. Chem. Mater. 2007; 19:6504.
3. Ramesh, K. Nanomaterials, Mechanics and Mechanisms. Baltimore, MD: Springer; 2009. Chapter 3.
4. Juliano R, Astriab-Fisher A, Falke D. Mol. Interv. 2001; 1:40–53. [PubMed: 14993337]
5. Carling P, Elliott DJ, Robson CN, Leung HY, Rajan P. Discov. Med. 2009; 8:74–80. [PubMed: 19788872]
6. Taylor J, Dean NM. Curr. Opin. Drug Discov. Devel. 1999; 2:147–151.

7. Fire A, Xu S, Montgomery MK, Kostas SA, Driver SE, Mello CC. Nature. 1998; 391:806–811. [PubMed: 9486653]
8. Drugs in development: Therapeutic Areas: Other. Isis Pharmaceuticals Inc. Web.
9. Roehr B. J. Int. Assoc. Physicians AIDS Care. 1998; 4:14–16. [PubMed: 11365956]
10. Geary R, Henry SP, Grillone LR. Clin. Pharmacokinet. 2002; 41:255–260. [PubMed: 11978144]
11. Castanotto D, Rossi JJ. Nature. 2009; 457:426–433. [PubMed: 19158789]
12. Kubasiak, L.; Tomalia, DA. Amiji, M. Polymeric Gene Delivery, Principles and Applications. Boston, MA: CRC Press; 2004. Chapter 9.
13. Fortier M, Kent S, Ashdown H, Poole S, Boksa P, Luheshi GN. Am. J. Physiol. Regul. Integr. Comp. Physiol. 2004; 287:R759–R766. [PubMed: 15205185]
14. Wang Y, Cella M, Gilfillan S, Colonna M. J. Immunol. 2010; 184:2751–2755. [PubMed: 20164430]
15. Ewel C, Urba WJ, Kopp WC, Smith JW II, Steis RG, Rossio JL, Longo DL, Jones MJ, Alvord WG, Pinsky CM, Beveridge JM, McNitt KL, Creekmore SP. Cancer Res. 1992; 52:3005–3010. [PubMed: 1591717]
16. Drug Candidates:Ampligen. Hemispherx Biopharma, Inc. Web.
17. DeLong RK, Akhtar U, Sallee M, Parker B, Barber S, Zhang J, Craig M, Hickey AJ, Engstrom E. Biomaterials. 2009; 30:6451–6459. [PubMed: 19726081]
18. Sokolova V, Epple M. Angew Chem. 2008; 47:1382–1395. [PubMed: 18098258]
19. Wang H, Yang R, Yang L, Tan W. ACS Nano. 2009; 3:2451–2460. [PubMed: 19658387]
20. Murphy C, Gole AM, Stone JW, Sisco PN, Alkilany AM, Goldsmith EC, Baxter SC. Acc. Chem. Res. 2008; 41:1721–1730. [PubMed: 18712884]
21. Sivamani E, DeLong RK, Qu R. Plant Cell Rep. 2009; 28:213–221. [PubMed: 19015859]
22. Han G, Martin CT, Rotello VM. Chem. Biol. Drug Des. 2006; 67:78–82. [PubMed: 16492152]
23. Alkilany AM, Nagaria PK, Hexel CR, Shaw TJ, Murphy CJ, Wyatt MD. Small. 2009; 5:701–708. [PubMed: 19226599]
24. Wu Y, Phillips JA, Liu H, Yang R, Tan W. ACS Nano. 2008; 2:2023–2028. [PubMed: 19206447]
25. Zea C, Camci-Unal G, Pohl NL. Chem. Cent. J. 2008; 2:15. [PubMed: 18627619]
26. Millonig H, Pous J, Gouyette C, Subirana JA, Campos JL. J. Inorg. Biochem. 2009; 103:876–880. [PubMed: 19375803]
27. Hussain S, Javorina AK, Schrand AM, Duhart HM, Ali SF, Schlager JJ. Toxicol. Sci. 2006; 92:456–463. [PubMed: 16714391]
28. Gann H, Glaspell G, Garrad R, Wanekaya A, Ghosh K, Cillessen L, Scholz A, Parker B, Warner M, DeLong RK. J. Biomed. Nanotechnol. 2010; 6:37–42. [PubMed: 20499830]
29. Kukowska-Latallo J, Bielinska AU, Johnson J, Spindler R, Tomalia DA, Baker JR Jr. Proc. Natl. Acad. Sci. USA. 1996; 93:4897–4902. [PubMed: 8643500]
30. Sakthivel T, Florence A. Drug Deliv. Technol. 2003; 3:73–78.
31. Nori A, Kopecek J. Adv. Drug Deliv. Rev. 2005; 28:609–636. [PubMed: 15722167]
32. Wolinsky J, Grinstaff M. Adv. Drug Deliv. Rev. 2008; 60:1037–1055. [PubMed: 18448187]
33. DeLong RK, Stephenson K, Loftus T, Fisher M, Alahari S, Nolting A, Juliano RL. J. Pharm. Sci. 1997; 86:762–764. [PubMed: 9188063]
34. Maiti P, Çagın T, Wang G, Goddard WA III. Macromolecules. 2004; 37:6236–6254.
35. Orberg M, Schillen K, Nylander T. Biomacromolecules. 2007; 8:1557–1563. [PubMed: 17458932]
36. Zhou J, Wu J, Hafdi N, Behr JP, Erbacher P, Peng L. Chem. Commun. 2006:2362–2364.
37. Kang H, DeLong RK, Fisher MH, Juliano RL. Pharm. Res. 2005; 22:2099–2106. [PubMed: 16184444]
38. Parimi S, Barnes TJ, Callen DF, Prestidge CA. Biomacromolecules. 2010; 11:382–389. [PubMed: 20038138]
39. Hong S, Bielinska AU, Mecke A, Keszler B, Beals JL, Shi X, Balogh L, Orr BG, Baker JR Jr, Banaszak Holl MM. Bioconjugate Chem. 2004; 15:774–782.

40. Wang W, Xiong W, Wan J, Sun X, Xu H, Yang X. Nanotechnology. 2009; 20:105103. [PubMed: 19417510]
41. DeLong RK, Reynolds CM, Malcolm Y, Schaeffer A, Severs T, Wanekaya A. Nanotechnology, Science and Applications. 2010; 3:53–63.
42. Cavaluzzi M, Borer PN. Nucleic Acids Res. 2004; 32:e13. [PubMed: 14722228]
43. Greene J, Alderfer J, Tazawa I, Tazawa S, Ts'o P, O'Malley J, Carter WA. Biochem. 1978; 17:4214–4220. [PubMed: 708705]
44. Zeta potential measurements using laser Doppler electrophoresis (LDE). Malvern Instruments Ltd. Web.
45. Puebla I, Esseghir S, Mortlock A, Brown A, Crisanti A, Low W. Journal of Biotechnology. 2003; 105:215–226. [PubMed: 14580793]
46. Bell H, Kimber W, Li M, Whittle I. NeuroReport. 1998; 9:793–798. [PubMed: 9579667]
47. Xing R, Liu G, Quan Q, Bhirde A, Zhang G, Jin A, Bryant LH, Zhang A, Liang A, Eden HS, Hou Y, Chen X. Chem Commun (Camb). 2011; 47(44):12152–12154. [PubMed: 21991584]
48. Davis M, Zuckerman J, Choi C, Seligson D, Tolcher A, Alabi C, Yen Y, Heidel J, Ribas A. Nature. 2010; 464:1067–1070. [PubMed: 20305636]

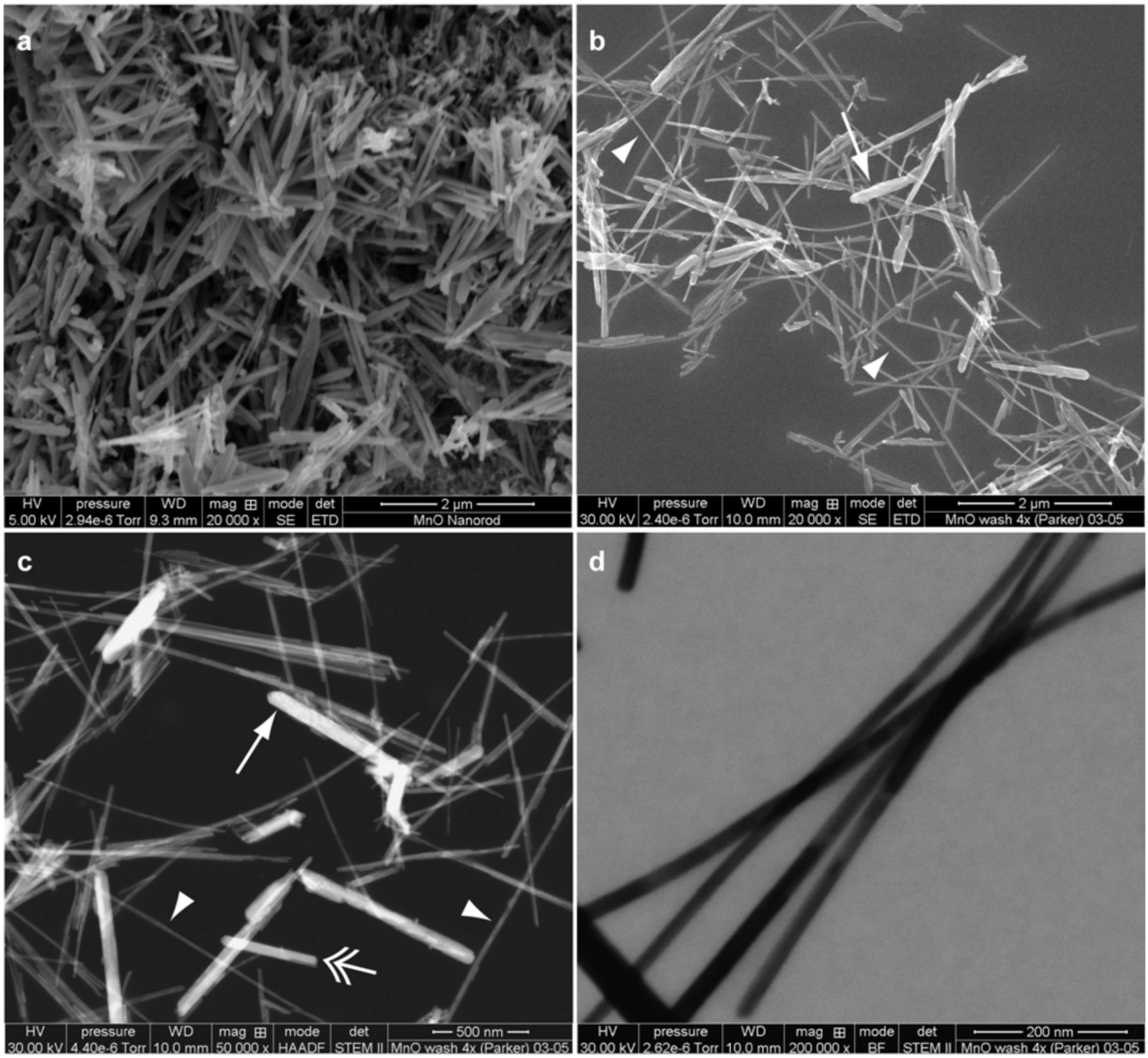

Figure 1.

Morphology of MnO nanorods. (a) SE image of unwashed MnO powder. Bar, 2 µm. (b) SE image of washed MnO nanorods dispersed on a silicon nitride substratum. Arrow indicates a large spatula; arrowheads indicate filaments. Bar, 2 µm. (c) STEM-HAADF image of washed nanorods dispersed on a silicon nitride substratum. Arrow indicates a large spatula; double arrow indicates a small spatula; arrowheads indicate filaments. Bar, 500 nm. (d) STEM-BF image of washed filaments at high magnification dispersed on a silicon nitride substratum. Bar, 200 nm. STEM, scanning transmission electron microscopy; HAADF, high-angle annular dark-field image mode; BF, bright field image mode.

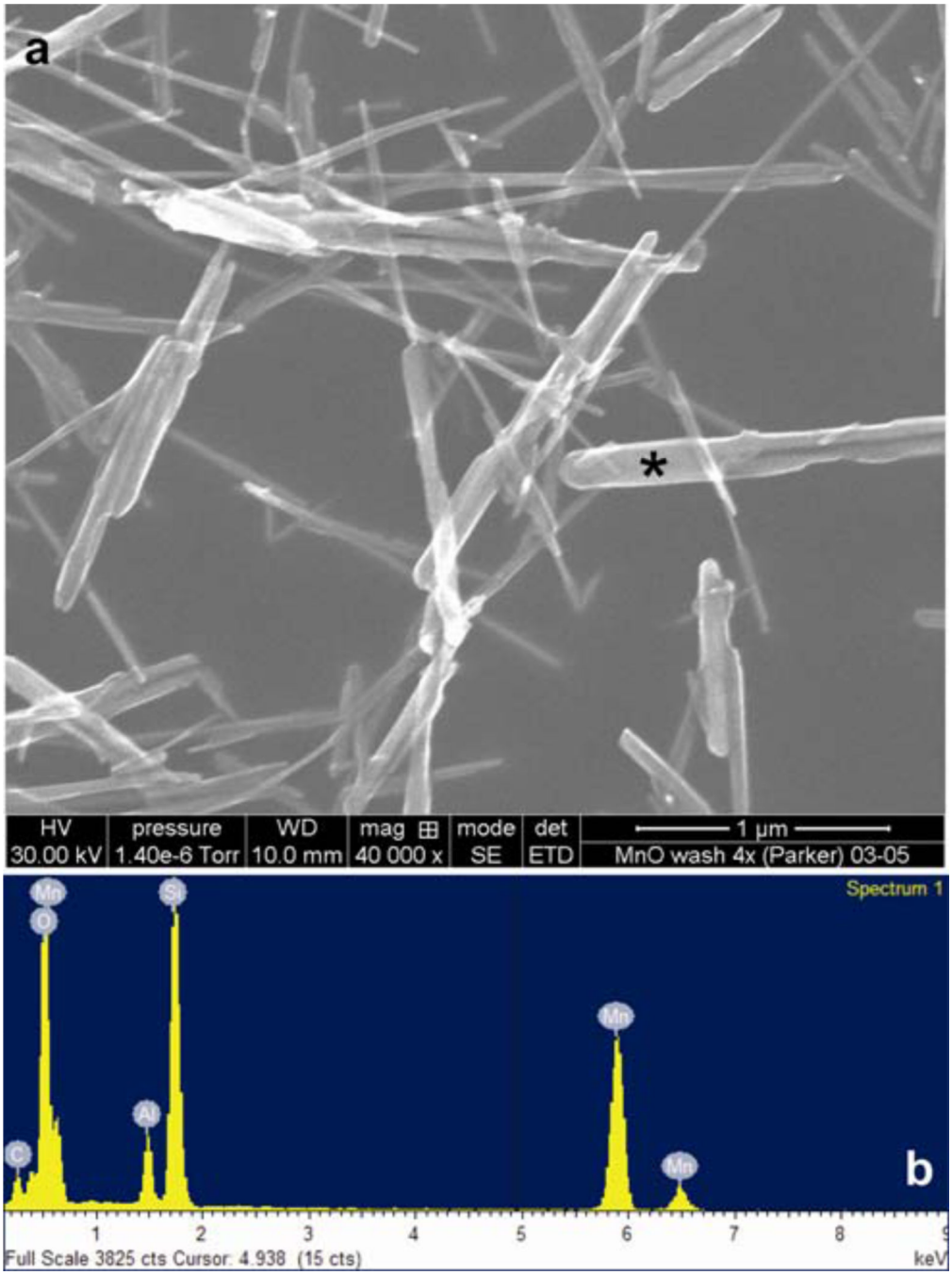

Figure 2.

EDX of MnO nanorods. (a) SE image of washed MnO nanorods dispersed on a silicon nitride substratum. Bar, 1 µm. (b) EDX qualitative spectrum generated from the point on a single nanorod indicated by an asterisk in (a). Energy peaks labeled Mn and O are derived from the designated nanorod; Al, specimen holder; Si and N (not labeled), support substratum. Mn, manganese; O, oxygen; Al, aluminum; Si, silicon.

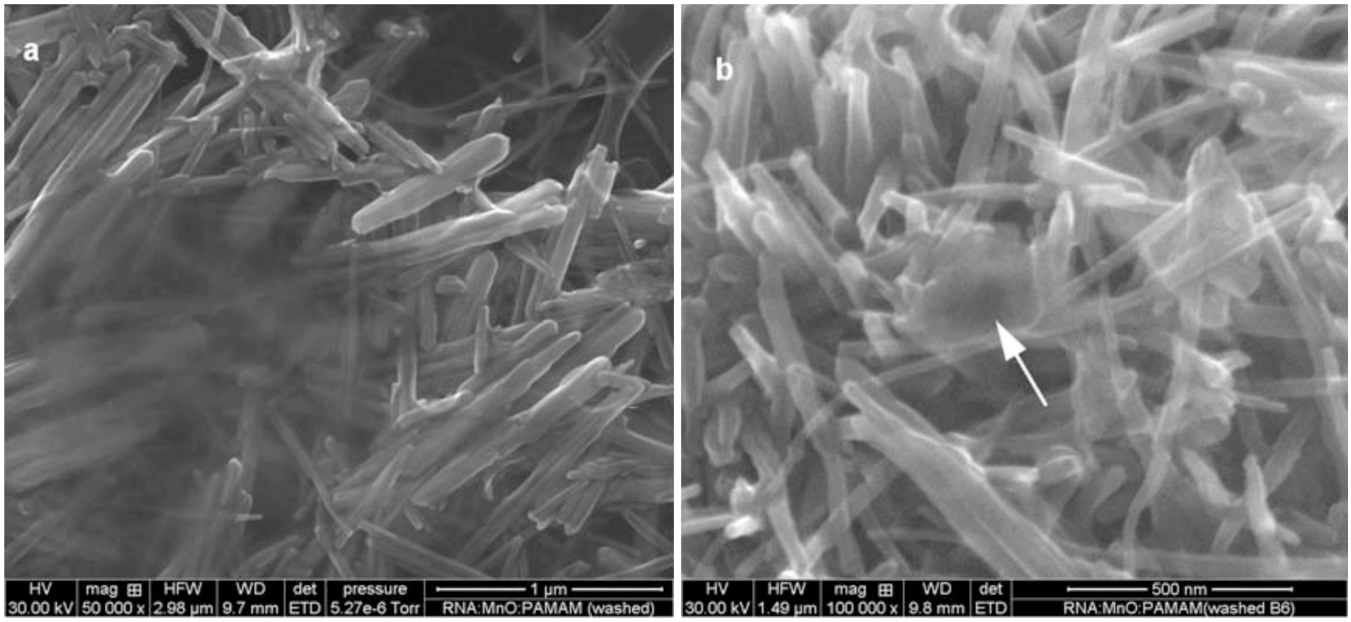

Figure 3.

Morphology of ethanol-washed, ternary RNA:PAMAM:MnO conjugates. (a) SE image of washed MnO nanorods embedded in the association matrix. Bar, 1 µm. (b) SE image of washed complex at high magnification ; arrow indicates discrete association matrix. Bar, 500 nm. SE, secondary electron image mode.

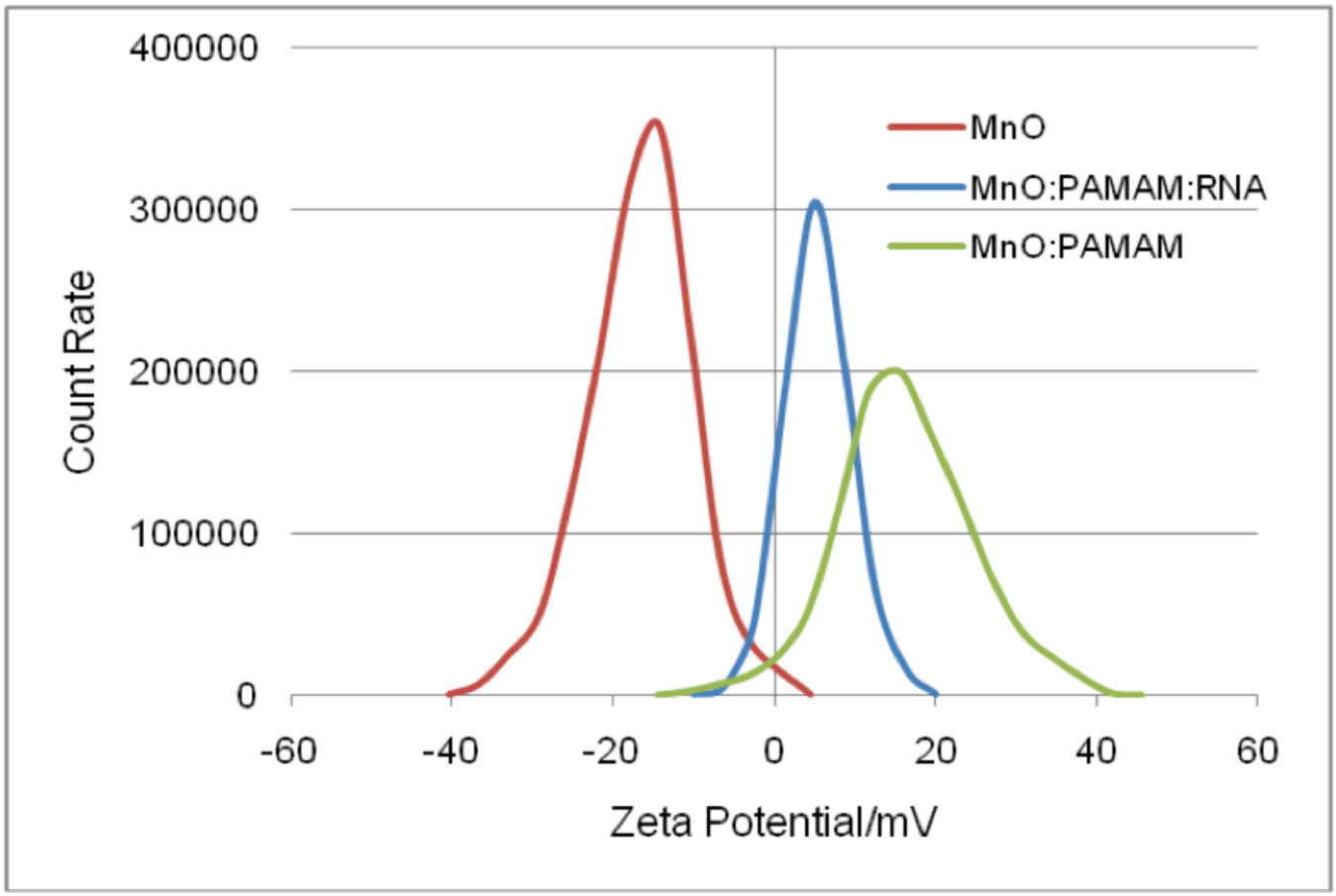

Figure 4.
RNA:PAMAM:MnO binding indicated by shifts in zeta potential. Controls were either MnO alone or PAMAM:MnO. The samples with PAMAM, RNA and RNA:MnO showed no shift, and were removed from the figure for simplicity.

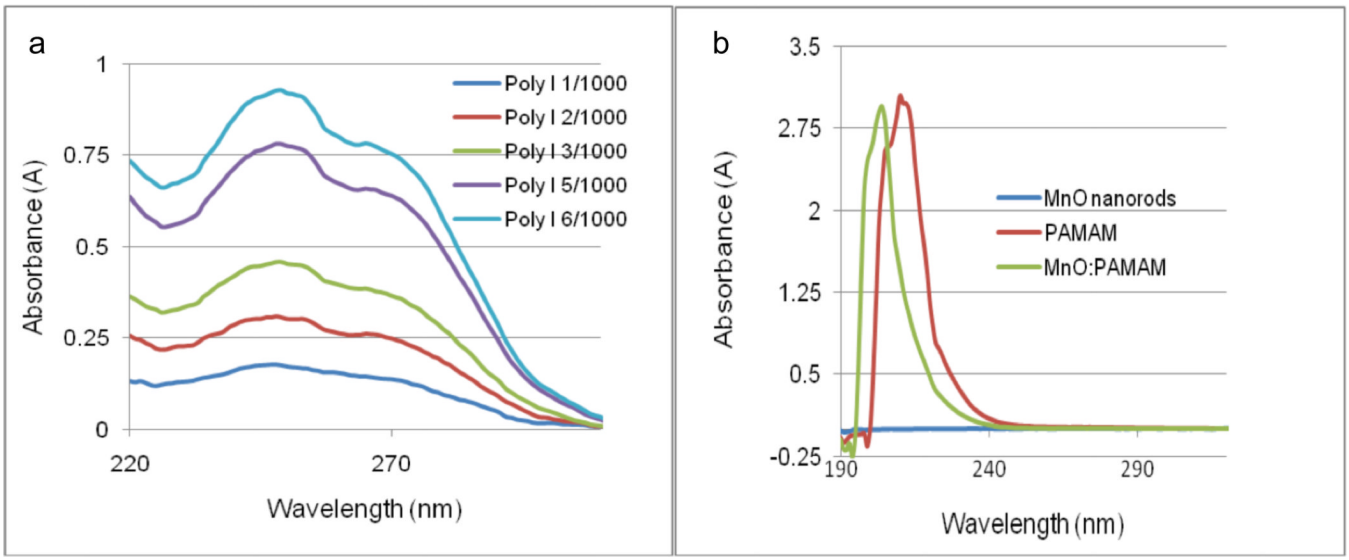

Figure 5.

UV spectra of (a) Poly I:C concentration gradient showing inosine UV absorbance peak at 248 nm and cytidine peak near 270 nm; (b) MnO nanorods showing no UV absorbance. PAMAM and PAMAM:MnO UV spectra showing PAMAM absorbance peak around 210 nm and PAMAM:MnO absorbance peak circa 205 nm.

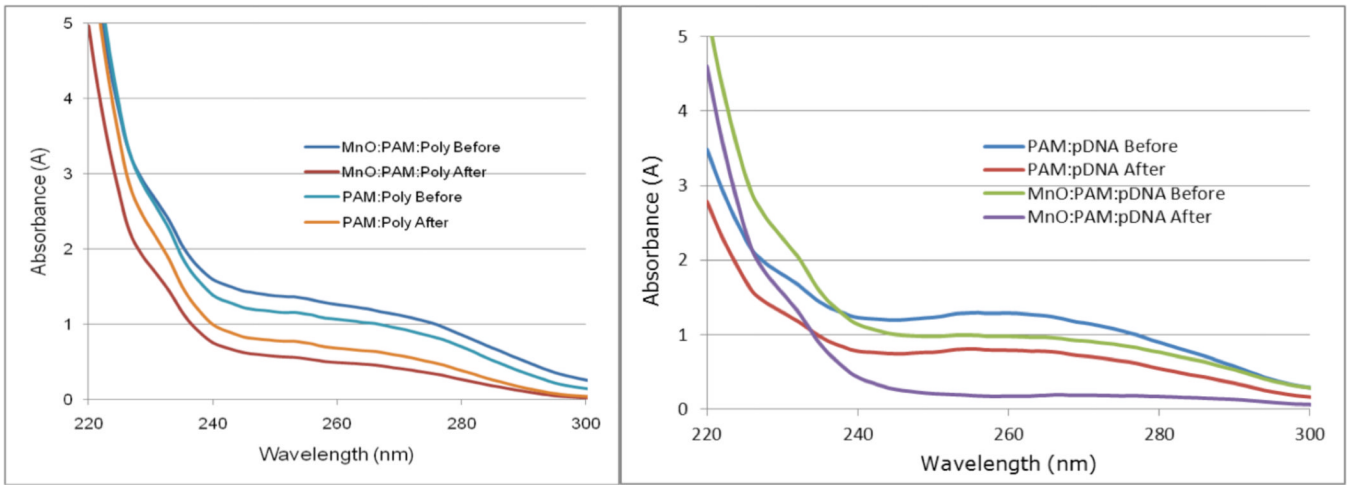

Figure 6.

UV spectroscopy of sedimentation assay. **(a)** A decrease in RNA UV absorbance after centrifugation indicates binding to, and sedimentation with, other molecules. A greater decrease in RNA absorbance is observed when MnO is present, indicating the RNA:PAMAM is forming a complex with the nanorods. Poly = poly I:C RNA. **(b)** A decrease in pDNA UV absorbance after centrifugation also indicates binding to, and sedimentation with, other molecules. A greater decrease in pDNA absorbance is observed when MnO is present, indicating the pDNA:PAMAM is forming a complex with the nanorods. The UV spectrum from RNA, pDNA, and PAMAM alone are the same before and after centrifugation, therefore they were excluded from Figure 6 for simplicity.

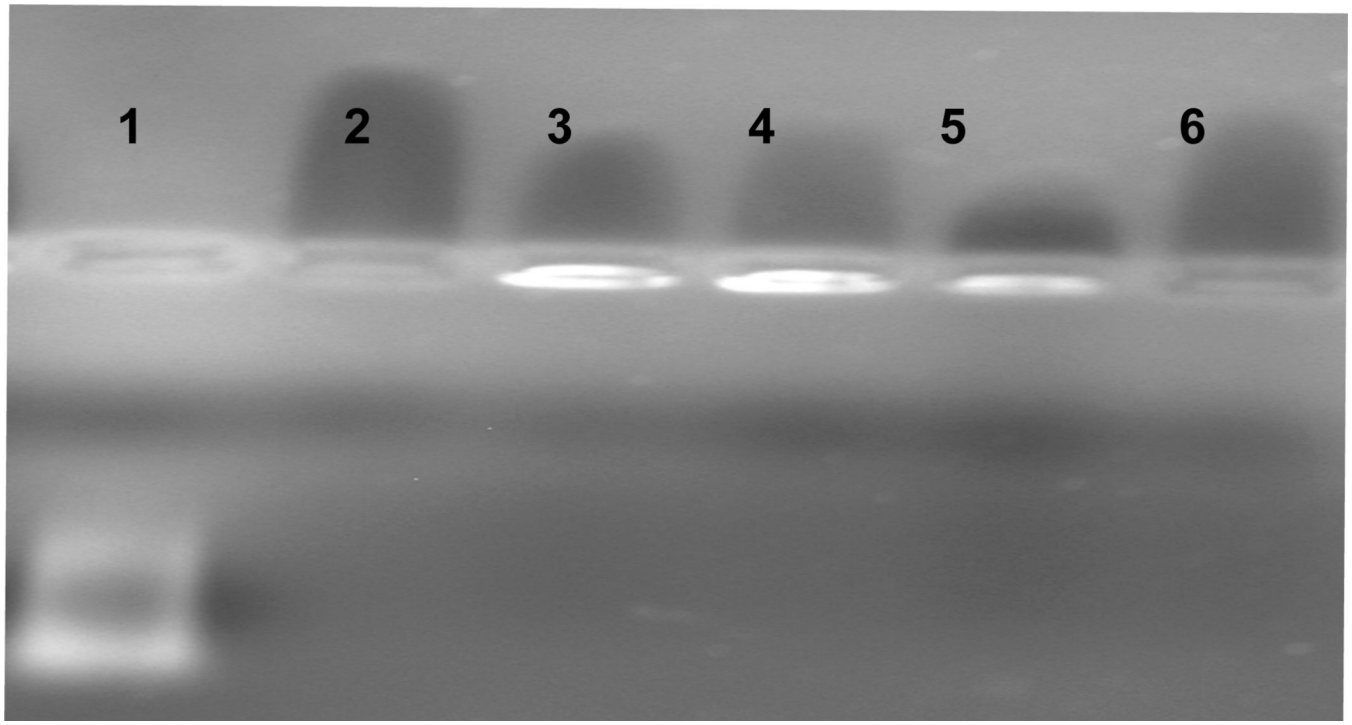

Figure 7.
Gel shift assay using 2% agarose gel electrophoresis showing that RNA migration is inhibited when combined with PAMAM and PAMAM:MnO complexes. Lanes (left to right): 1, RNA; 2, PAMAM; 3, RNA:PAMAM; 4, RNA:PAMAM; 5, RNA:PAMAM:MnO; 6, PAMAM:MnO.

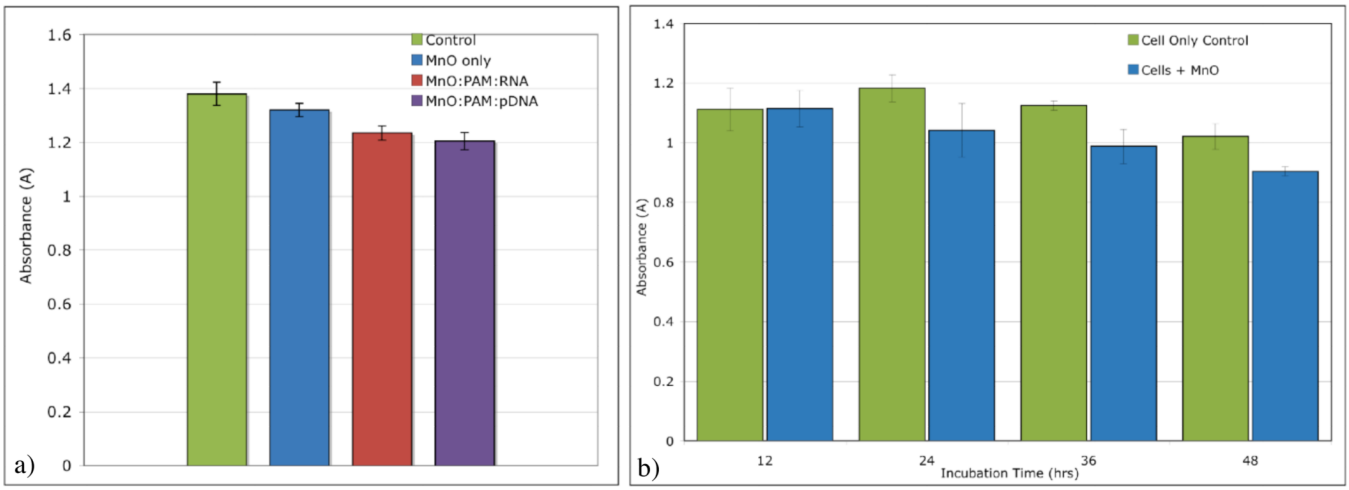

Figure 8.

MTT assay to determine ability of HeLa cells to reduce yellow MTT into purple formazan (a) after 24 hour incubation with MnO only, RNA:PAMAM:MnO, and pDNA:PAMAM:MnO; (b) after incubation with MnO only for 12, 24, 36, and 48 hours. For both assays, there were only minor decreases in metabolic activity, as compared to the cell only control. Error bars for both figures were plotted using standard error.

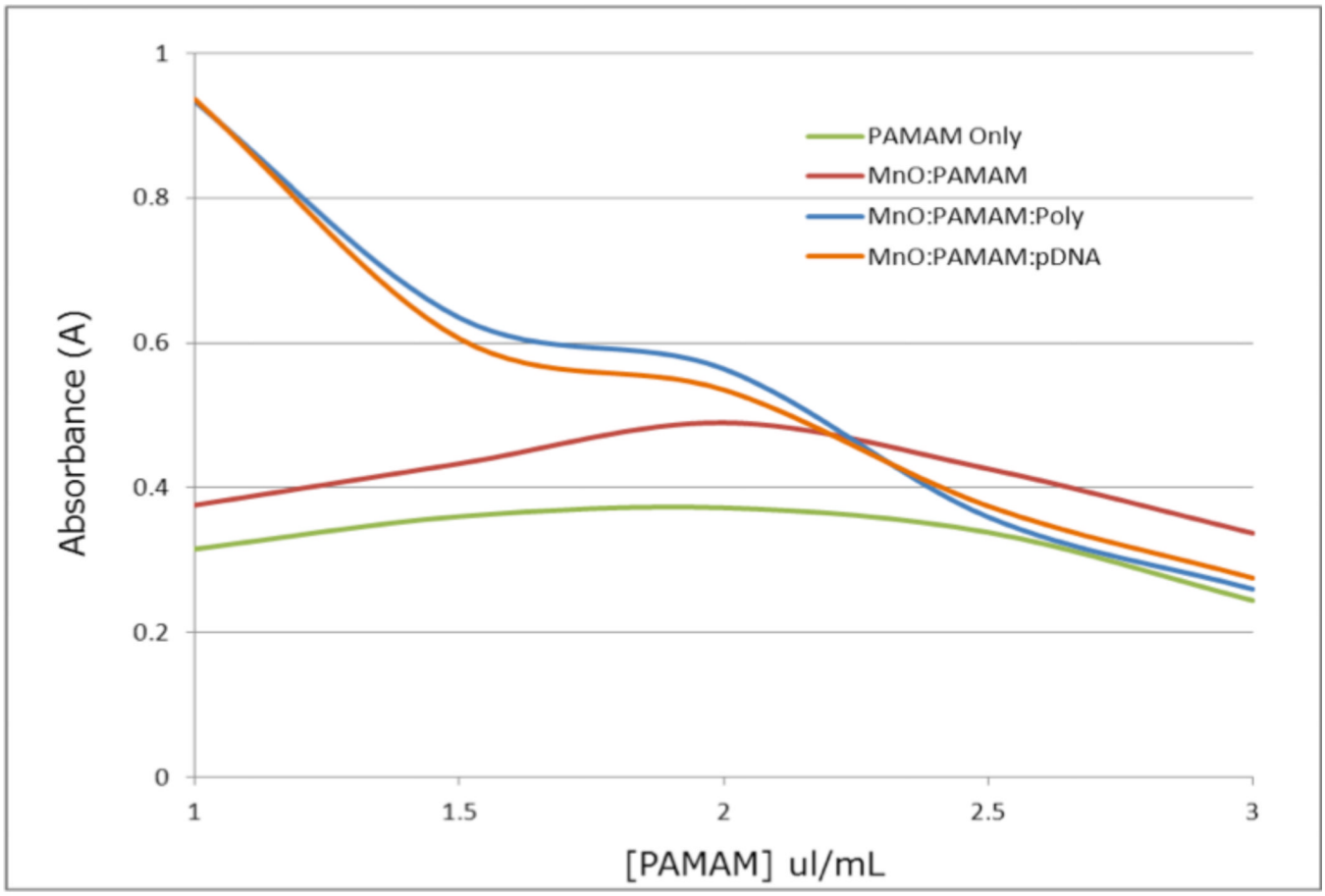

Figure 9.

MTT to analyze the effects of varying concentrations of PAMAM on the metabolic activity of HeLa cells. The cells incubated with PAMAM only showed the least amount of metabolic activity, while a definite increase was observed in those cells incubated with PAMAM:MnO. The cells incubated with the RNA: PAMAM:MnO and pDNA:PAMAM:MnO complexes proved to be significantly more metabolically active than the other two samples.

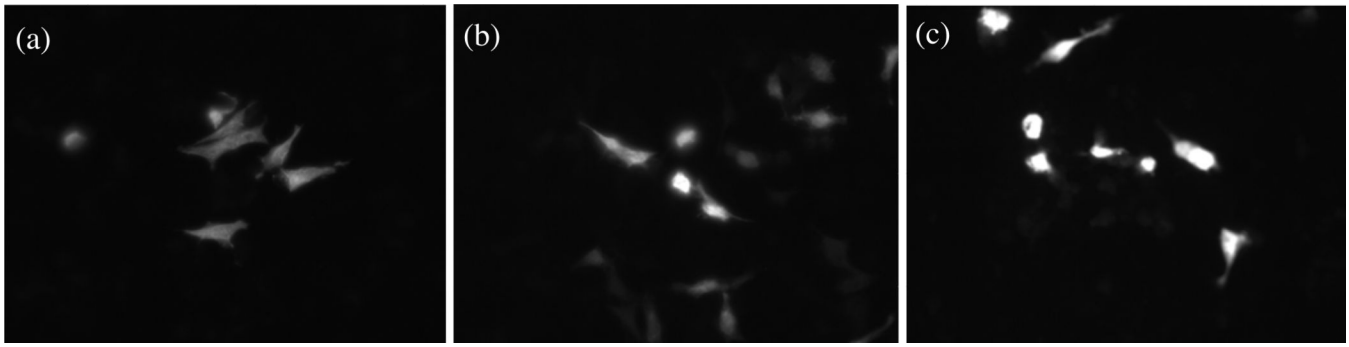

Figure 10.

Transfection assay using pDNA expressing GFP reporter gene. The transfection of HeLa cells was performed with the following samples: PAMAM:MnO, which served as the negative control and demonstrated no fluorescent cells and was therefore excluded from this figure; (a) pDNA:PAMAM only, which displayed only minor fluorescence; (b) Lipofectamine:pDNA, which served as the positive control; and (c) pDNA:PAMAM:MnO, which showed significantly more fluorescence than the other samples. Representative images from each group are shown here.

Table 1

Average Zeta Potential Measurements for Figure 4

	DLLS Zeta Potential Shift
MnO alone	− 16.5 mV ± 0.17
MnO:PAMAM	16.3 mV ± 0.75
MnO:PAMAM:RNA	5.4 mV ± 0.68

Table 2

Sedimentation Assay UV Spectroscopy Results Showing Changes in Nucleic Acid Absorbance and Nucleic Acid Concentration of the Supernatant before and after Centrifugation When Combined with PAMAM Alone or PAMAM:MnO Nanorods[a]

Sedimentation of RNA and pDNA by PAMAM and PAMAM:MnO

	RNA:PAMAM	RNA:PAMAM:MnO	pDNA:PAMAM	pDNA:PAMAM:MnO
A260 Before	1.067	1.264	1.290	0.979
A260 After	0.687	0.493	0.790	0.173
A280 Before	0.701	0.861	0.899	0.765
A280 After	0.389	0.268	0.545	0.170
[Nucleic Acid] Before	42.7 μg/mL	50.6 μg/mL	64.5 μg/mL	49.0 μg/mL
[Nucleic Acid] After	27.5 μg/mL	19.7 μg/mL	39.5 μg/mL	8.6 μg/mL
% Sedimented	47.7	71.4	46.7	81.8

[a]Data are from Figure 6; sedimented values (%) are averages from multiple runs not shown in Figure 6.